Carbon nitride-based light-driven microswimmers with intrinsic photocharging ability

Varun Sridhar[a,1], Filip Podjaski[b,1], Julia Kröger[b,c], Alberto Jiménez-Solano[b], Byung-Wook Park[d], Bettina V. Lotsch[b,c,2], and Metin Sitti[a,e,f,g,2]

[a]Physical Intelligence Department, Max Planck Institute for Intelligent Systems, 70569 Stuttgart, Germany; [b]Nanochemistry Department, Max Planck Institute for Solid State Research, 70569 Stuttgart, Germany; [c]Department of Chemistry, University of Munich (LMU), 81377 Munich, Germany; [d]Department of Chemical Engineering, Youngstown State University, Youngstown, OH 44555; [e]School of Medicine, Koç University, 34450 Istanbul, Turkey; [f]School of Engineering, Koç University, 34450 Istanbul, Turkey; and [g]Institute for Biomedical Engineering, ETH Zurich, 8092 Zurich, Switzerland

Edited by John A. Rogers, Northwestern University, Evanston, IL, and approved August 24, 2020 (received for review April 17, 2020)

Controlling autonomous propulsion of microswimmers is essential for targeted drug delivery and applications of micro/nanomachines in environmental remediation and beyond. Herein, we report two-dimensional (2D) carbon nitride-based Janus particles as highly efficient, light-driven microswimmers in aqueous media. Due to the superior photocatalytic properties of poly(heptazine imide) (PHI), the microswimmers are activated by both visible and ultraviolet (UV) light in conjunction with different capping materials (Au, Pt, and SiO_2) and fuels (H_2O_2 and alcohols). Assisted by photoelectrochemical analysis of the PHI surface photoreactions, we elucidate the dominantly diffusiophoretic propulsion mechanism and establish the oxygen reduction reaction (ORR) as the major surface reaction in ambient conditions on metal-capped PHI and even with TiO_2-based systems, rather than the hydrogen evolution reaction (HER), which is generally invoked as the source of propulsion under ambient conditions with alcohols as fuels. Making use of the intrinsic solar energy storage ability of PHI, we establish the concept of photocapacitive Janus microswimmers that can be charged by solar energy, thus enabling persistent light-induced propulsion even in the absence of illumination—a process we call "solar battery swimming"—lasting half an hour and possibly beyond. We anticipate that this propulsion scheme significantly extends the capabilities in targeted cargo/drug delivery, environmental remediation, and other potential applications of micro/nanomachines, where the use of versatile earth-abundant materials is a key prerequisite.

carbon nitrides | light-driven | microswimmers | photocharging | solar battery

Microswimmers are micrometer-scale wireless machines that are propelled in fluids by converting energy made available in their surroundings, such as chemical bonds, light, and magnetic and acoustic fields (1, 2). Such autonomous propulsion makes microswimmers highly attractive, active microdevices in various biomedical and environmental applications (3). While the use of sacrificial reagents can provide chemical energy for propulsion, it requires their continuous supply (4) and makes directional control difficult. Light, however, is abundant and one of the most widely exploited "fuels" to propel microswimmers photocatalytically (5, 6), enabling temporally and spatially controlled motion, called phototaxis (7). Two light-driven propulsion mechanisms are possible for Janus microparticle-based microswimmers. The first mechanism is self-diffusiophoresis (8), which is induced by diffusion of catalytically converted species in solution due to the surface reactions of the photocatalyst or its capping material. The production of a concentration gradient of reduced and oxidized species leads to convection and spontaneous motion of the microswimmer along the gradient, enabling continuous propulsion (4, 9). The second mechanism is self-electrophoresis (8), which is characterized by the transfer of electrons between the different layers of the Janus photocatalyst, generating momentum transfer (propulsion) by the formation of an electric field, which is balanced by convection of charged species generated by surface redox reactions.

So far, many photoactive molecules and materials have been adapted to serve as light-driven microswimmers by decoration with electrocatalysts (6, 10). However, photocatalytic propulsion has mostly been realized with inorganic semiconductors, such as TiO_2 (1, 11–27). A transition to nature-inspired, organic microswimmers is thus of high interest, especially regarding potential improvements in biocompatibility, tunability, and cost (28). In recent years, organic semiconductors have become a prominent class of materials for (opto)electronics and photocatalysis (29–32), which renders them promising material candidates for microswimmers as well. Nevertheless, only a few examples of organic materials being used for light-driven self-diffusiophoretic or -electrophoretic propulsion have been reported (33, 34). They rely on agglomerated, melon-based "graphitic" carbon nitrides (CN_x), which consist of strictly alternating carbon and nitrogen atoms forming heptazine units that are linked by imide bridges to one-dimensional (1D) polymer chains. Among the most recent and most active hydrogen evolution photocatalysts is poly(heptazine imide) (PHI) (Fig. 1*A*) (32, 35), a 2D CN_x with intriguing photophysical properties (32): PHI has the ability to store photogenerated

Significance

Light-driven microswimmers offer prospects for autonomous microsystems. Understanding their surface catalytic processes responsible for propulsion is essential in tailoring them for specific applications. So far, photocatalytic microswimmers have been limited by the requirement of continuous illumination. Here, we report light-driven 2D carbon nitride-based Janus microswimmers, which show efficient propulsion in aqueous media not only during but also after illumination for about 30 min after 30 s prior illumination, due to so-called solar battery swimming. Contrary to the mainstream reports, we reveal oxygen reduction rather than hydrogen evolution being responsible for propulsion with alcohol fuels. Balancing reaction conditions, we report the realization of light-induced intrinsic charging of a microswimmer, enabling sustained ballistic propulsion in the dark through discharge of accumulated energy.

Author contributions: V.S., F.P., B.-W.P., B.V.L., and M.S. designed research; V.S., F.P., J.K., and A.J.-S. performed research; V.S., F.P., J.K., and A.J.-S. analyzed data; and V.S., F.P., B.V.L., and M.S. wrote the paper.

The authors declare no competing interest.

This article is a PNAS Direct Submission.

[1]V.S. and F.P. contributed equally to this work.

[2]To whom correspondence may be addressed. Email: b.lotsch@fkf.mpg.de or sitti@is.mpg.de.

This article contains supporting information online at https://www.pnas.org/lookup/suppl/doi:10.1073/pnas.2007362117/-/DCSupplemental.

First published September 21, 2020.

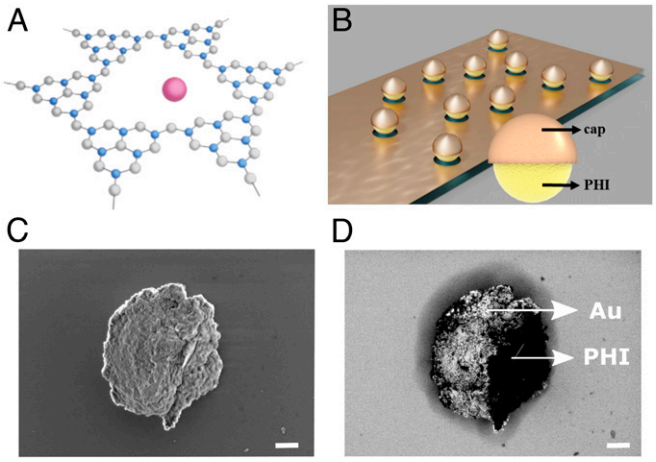

Fig. 1. Structure of poly(heptazine imide) (PHI)-based Janus microswimmers. (*A*) Chemical structure of PHI consisting of carbon (blue), nitrogen (gray), and hydrogen (omitted for clarity). Solvated potassium ions reside in structural pores (purple). (*B*) Schematic of the preparation of the PHI-based Janus microswimmers by directional sputtering of cap materials (Au, Pt, or SiO_2) on PHI microswimmers. (*C*) In-lens and corresponding backscattered electron (*D*) Scanning electron microscope (SEM) images of the spherical PHI–Au Janus microswimmers with the Au-capped side being on the left. The expected elemental contrast (Au brighter) is clearly visible in *D*. (Scale bar, 400 nm.)

electrons in a long-lived photo-reduced state for days after illumination is stopped, with a capacity ranging up to 96 C/g (35–37). These electrons can be discharged on-demand, i.e., by the time-delayed addition of a cocatalyst that reduces water to hydrogen. As a consequence, the light and dark reactions of photocatalysis can be decoupled to produce solar fuels under dark conditions, akin to the processes occurring in natural photosynthesis (37). This concept called "dark photocatalysis" can be extended to electrical charge transfer to realize new types of solar batteries (37, 38).

In this work, we investigate the light-induced propulsion of PHI Janus particle-based microswimmers with caps consisting of Au, Pt, and SiO_2, and we demonstrate that these properties can be exploited to realize efficient microswimmer propulsion not only in the presence, but also in the absence of light. Our findings reveal the light-induced surface catalytic processes and indicate that the reduction reaction, which is responsible for the microswimmer propulsion with alcohol donors in ambient conditions, is not the hydrogen evolution reaction (HER), but rather the oxygen reduction reaction (ORR), or more generally, the formation of reactive oxygen species (ROS), even when Pt or Au are used as cocatalysts. Under optimized conditions, our PHI-based Janus microswimmers move with comparable speeds of similar, melon type CN_x-based microswimmers, and we demonstrate propulsion with visible light only (33, 34).

Making use of the dual functionality of light absorption and charge storage, we further show that light-induced charging is possible in H_2O_2, enabling persistently enhanced propulsion after the illumination stopped, up to a duration of ∼30 times the initial illumination period, with some particles showing dark ballistic swimming for more than half an hour. This "solar battery swimming" concept potentially enables new micro/nanomachine applications, such as drug delivery and environmental remediation under dark conditions, e.g., inside the human body, and in situ power supply for micro/nanomachines.

Results and Discussion

PHI-based Janus microswimmers were obtained by sonication of the bulk material and subsequent separation of particle sizes by centrifugation (*Materials and Methods*). The largest fraction is deposited on a substrate and caps are evaporated on top directionally to form Janus microswimmers, as illustrated in Fig. 1*B*. Scanning electron microscopy (SEM) analysis revealed near-spherical shapes with a diameter of 1 to 3 μm (Fig. 1*C*) and the backscattered electron image showing the gold content in Fig. 1*D*. The obtained microswimmers are not completely spherical, since they represent agglomerates of PHI nanoparticles that are separated after bulk synthesis resulting in imperfectly half-capped Janus microswimmers. Therefore, the fabricated Janus microstructures are also irregularly shaped Janus microstructures, as shown in *SI Appendix*, Fig. S1. In order to check whether and how these microswimmers can be moved in aqueous conditions, an additional thin Ni layer is deposited in between the PHI and the cap to enable magnetic control (for more details, see *SI Appendix*, *Supplementary Note 1*). The PHI–Ni–Pt microswimmers follow the direction of the applied magnetic field as shown in *SI Appendix*, Fig. S3 and in Movie S1. Their speed is 12.1 ± 0.3 μm/s at an applied field of 8 mT, which is comparable to inorganic TiO_2-based microswimmers of similar size (13.3 ± 0.4 μm/s) (39).

To establish the optical properties of the PHI–Pt microswimmers, the absorptance is measured (*SI Appendix*, Fig. S4). The absorption edge of ∼450 nm is similar to bulk and nanostructured PHI (38), but with an increased background, which is attributed to the metal cap. Hence, light in the blue and UV part of the solar spectrum can be absorbed and used for catalytic conversion to propel the microswimmer. The organic semiconductor PHI has a conduction band (CB) edge well negative of the reversible hydrogen electrode (RHE), approximately −500 mV versus normal hydrogen electrode (NHE), and a valence band (VB) as positive as +2.2 V vs. NHE, allowing PHI to drive multiple redox reactions, such as HER, ORR, and water oxidation (37, 38, 40, 41). The type of cocatalyst, i.e., the material used for the Janus cap, and the choice of fuel are crucial design parameters for optimized phototactic applications. To study the swimming behavior of the PHI microswimmers, we used Pt, Au, and SiO_2 caps and illuminated the Janus microswimmers with visible and UV light.

Swimming Behavior in Water and Water–Alcohol Mixtures. In order to enable the HER on PHI, an active catalyst such as Pt or Au is required owing to the high intrinsic overpotential of carbon nitrides for HER (38). We hence illuminated the corresponding Janus microswimmers and measured their mean square displacement (MSD) in deionized (DI) water. On short timescales (∼1 s), the motion is ballistic and hence mostly linear. The displacement is significantly enhanced by UV light, as shown in Fig. 2*A* for all Janus microswimmers, along with a control experiment using the microscope light only. The mean speed can be extracted from the average slope. On longer timescales (∼15 s), the speed of the UV-illuminated PHI–Pt microswimmers are 10.4 ± 0.6 μm/s, while PHI–Au microswimmers swam with 9.1 ± 0.6 μm/s (13% slower), as shown in Fig. 2*B* (*Left* side). Interestingly, the PHI–SiO_2 microswimmers were propelled at almost the same speed (8.6 ± 0.7 μm/s), without having a redox-active cap. Importantly, however, this observation excludes HER as the source of self-diffusiophoresis, owing to the large overpotential of the HER on the PHI surface as shown in an earlier work (38). Hence, another reductive process must be operative, which will be discussed further below. However, these results show that the capped PHI microswimmers can move even in the absence of a dedicated fuel and indicate that the propulsion process is almost independent of the capping material when only water is used as fuel.

In order to increase the propulsion activity of the microswimmers, which is limited by the sluggish kinetics of the hole extraction in pure water, alcohols like methanol (MeOH) or 4-methyl

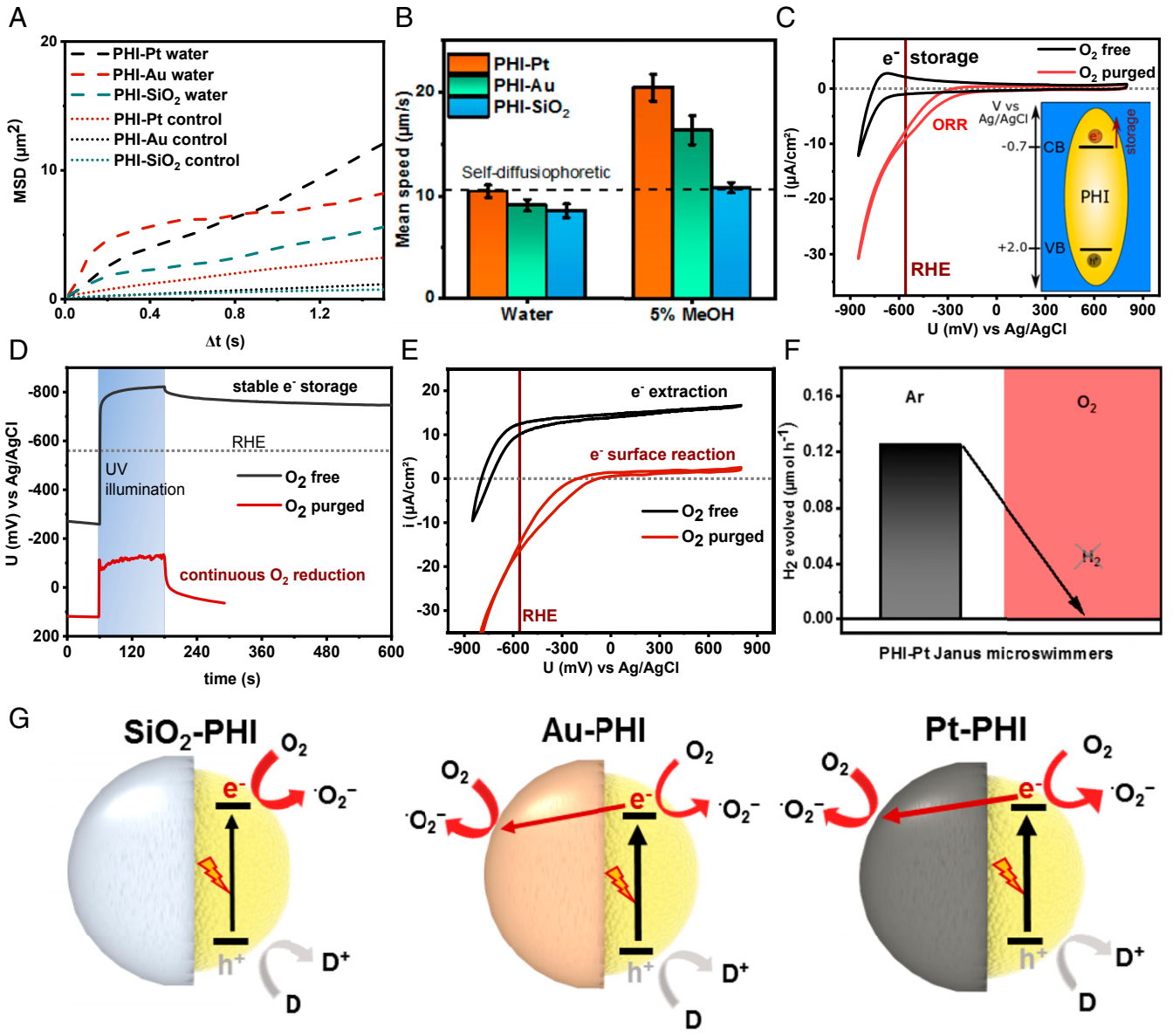

Fig. 2. Characterization of the swimming behavior of different PHI-based Janus microswimmers in water and with alcohol. (*A*) Two-dimensional mean-square-displacement (MSD) swimming trajectory data as a function of the time interval for the PHI–Pt, PHI–Au, and PHI–SiO_2 microswimmers in DI water with UV light on short timescales (~1 s) and the control experiment in the dark (dotted lines). (*B*) Average ($n = 25$) mean speed of the UV light-driven PHI–Pt, PHI–Au, and PHI–SiO_2 microswimmers on longer timescales (~15 s) in water and with methanol (MeOH) (Movies S2 and S3). (*C–E*) Electrochemical characterization of exfoliated PHI sheets deposited on FTO. (*C*) Current–voltage measurement (CV) showing reversible electron storage and release above RHE upon cathodic cycling in O_2-free electrolyte (black line) and the oxygen reduction reaction (ORR) (red line) occurring positive of the RHE under oxygen-containing conditions, thus hindering charge accumulation and storage. The inset illustrates the positions of the valence band (VB) and conduction band (CB), where electron storage occurs. (*D*) Open circuit potential (OCP) measurements for both conditions in the dark, under and after UV illumination. (*E*) CV showing potential-dependent electron extraction current under UV illumination in the presence of an electron donor (MeOH), providing a measure of the charges available for diffusiophoresis under ambient and O_2-free conditions. (*F*) Hydrogen evolution measurement of PHI–Pt Janus microswimmers in degassed water containing 10% MeOH (*Left*) and evidence of the absence of hydrogen production in oxygen-containing conditions (*Right*) (see *SI Appendix*, Fig. S10 for the same finding on other semiconductor–metal combinations). (*G*) Schematics illustrating the major and minor light-induced redox reactions on both sides of the three PHI-based Janus microswimmers. Reduction reactions (driven by electrons) are indicated by a red arrow (with Au and Pt caps), whereas the oxidation (driven by photogenerated holes) is highlighted in gray.

benzyl alcohol were added, which have been shown to reduce the lifetime of photogenerated holes on PHI efficiently to significantly below 3 μs (42). With 5% MeOH added as a hole extraction fuel, the mean speed of the PHI–Pt microswimmers is almost doubled to 20.4 ± 1.3 μm/s (Fig. 2*B*, *Left* side). Increasing the MeOH concentration to 10% yields comparable speeds of 20.6 ± 0.9 μm (*SI Appendix*, Fig. S5). Hence, a saturation of the rate-limiting donor reaction can be estimated at 5% MeOH already.

Due to the biocompatibility of Au, its use as catalytically active cap material instead of Pt is also of interest, especially for biomedical applications (43, 44). Again, the speed of PHI–Au microswimmers is found to be almost doubled to 16.3 ± 1.4 μm/s with 5% MeOH, i.e., 20% less than that observed with PHI–Pt microswimmers. The overall similar mean speed of both types of metal Janus microswimmers indicates similar surface reaction kinetics, despite the distinctly different catalytic activities of Pt

and Au toward HER. The mean speed of SiO_2-capped microswimmers, however, increased only slightly upon addition of the alcohol (10.7 ± 0.5 μm/s with 5% MeOH, +25%) and remains significantly below that of the metal-capped Janus microswimmers (47% less that Pt–PHI). The catalytic reactions that are responsible for propulsion hence rely on the complex interplay of both sides of the Janus particle.

The swimming speed of the PHI Janus microswimmers is approximately two times larger than for inorganic TiO_2–Au microswimmers with 1- to 2-μm diameter under the same illumination and donor conditions, which is 9.2 ± 0.5 μm/s (39), and of similar speed as TiO_2–Pt microswimmers (8.9 μm/s) in DI water under the same illumination conditions (1.9 W/cm^2) (45). The PHI microswimmers are capable of active propulsion at similar speed as melon-type CN_x-based microswimmers (33). The efficient use of light by PHI microswimmers can be attributed to the high quantum yield of the surface reaction occurring on PHI in comparison to other organic photocatalysts, possibly originating from the more efficient hole transfer to the alcohol (42), less recombination-active trap states in the material (46), and from better charge separation efficiencies at the metal–semiconductor junction in the Janus particle.

Photoelectrochemical Characterization with Water and Methanol as Donor. To elucidate the nature of the electrochemical reactions occurring on the surface of PHI, we studied the photoelectrochemical (PEC) properties of PHI. To this end, exfoliated PHI nanosheets are deposited on a conductive fluorine-doped tin oxide glass (FTO) substrate and characterized electrochemically in the dark and with 15 mW/cm^2 during UV illumination at 365 nm from the same light source used for the swimming experiments, both in the presence and absence of oxygen (Fig. 2 *C*–*E*). As can be seen in the cyclic voltammogram (CV) in Fig. 2*C*, anodic cycling of PHI in oxygen-free conditions (black curve) in the dark leads to a reversible electron storage and retraction process (schematics in the inset), which occurs at approximately −700 mV vs. Ag/AgCl, well negative of the RHE, thus enabling electron transfer to a cocatalyst and HER, in principle. Illumination in the presence of a donor also enables stable electrochemical electron storage (38) and yields a negative open circuit potential (OCP) of approximately −800 mV vs. Ag/AgCl in the absence of O_2 (Fig. 2*D*, black curve), even after illumination. These photogenerated electrons can be extracted by applying more positive potentials, leading to photocurrents of 10 to 15 μA/cm^2 (Fig. 2*E*, black curve). However, the situation is distinctly different in the presence of oxygen (red curves); here, PHI neither shows electron storage upon electrical charging (Fig. 2*C* and *SI Appendix*, Fig. S6 for different conditions) nor by photo-charging (Fig. 2*D* and *SI Appendix*, Fig. S7), which impedes electrical charge extraction, as shown in Fig. 2*E*. In other words, the ORR takes place predominantly at potentials of approximately −200 mV vs. Ag/AgCl or more positive, i.e., well positive of the RHE and, hence, preferentially over the HER. Consequently, the accumulation of (photogenerated) electrons in the CB is impeded by rapid electron transfer to the oxygen present in solution, reducing it to water or forming ROS that then react further, as discussed in *SI Appendix*, *Supplementary Note 2*, and as observed on other semiconductors (47).

In the case of inert SiO_2-capped Janus microswimmers, all photoelectrons are transferred to oxygen, and hence, it can be assumed that self-diffusiophoretic propulsion occurs from the PHI hemisphere only (Fig. 2*G*). For Pt- or Au-capped Janus microswimmers, the same mechanism is possible, in principle, and probably dominates when no donor is present, since all swimming speeds are comparable (*SI Appendix*, *Supplementary Note 3* and Fig. S8). Since significantly increased swimming speeds have been observed only on metal-capped Janus microswimmers with MeOH, i.e., when the hole extraction from PHI is fast and not rate limiting, the cap must be active for charge separation and also drive a surface reaction under these conditions. Charge carrier separation at the metal–semiconductor interface decreases recombination and simultaneously enables reduction reactions on both Janus hemispheres. Internal electron transfer from PHI to the metal cap hence adds self-electrophoresis as a likely propulsion mechanism to the MSD (Fig. 2*G*).

To obtain a full picture of the reduction products, we studied the gas formation of Pt-capped PHI Janus microswimmers. Illumination in the presence of MeOH under oxygen-free conditions evidences the accumulation of hydrogen in the headspace of a sealed reactor, as shown in Fig. 2*F*, black bar, for the full spectrum of a xenon lamp and *SI Appendix*, Fig. S9 for comparison to air mass filter (AM 1.5 G) and UV illumination conditions used to study the swimming (see *SI Appendix*, *Supplementary Note 4* for discussion). However, if oxygen is not removed from the suspension, no hydrogen is observed over 23 h with the same Janus particle suspension. The same observation is made with photo-deposited Pt or Au on both PHI and TiO_2 (anatase), where HER is only observed when oxygen was removed from the suspension (*SI Appendix*, Fig. S10). ORR occurs in ambient conditions with water and/or alcohol donors present with Au and Pt used as reduction catalysts, which is evidenced on both PHI and TiO_2. Therefore, it can be expected that the preference of the ORR over HER in the presence of oxygen can be generalized. We thus conclude that the fastest swimming Pt-capped and Au-capped microswimmers are dominantly active for ORR/ROS formation in ambient conditions, which is happening on both sides as long as oxygen is present in the environment.

Swimming with H_2O_2 as Fuel. We also studied the active propulsion in H_2O_2, a widely used fuel for microswimmers. Since noble metals such as Pt also catalyze the decomposition of H_2O_2 in the absence of light, this fuel is commonly used for microswimmer propulsion without light (4). H_2O_2 is redox amphoteric, i.e., it can be both oxidized and reduced (*SI Appendix*, *Supplementary Note 5*), making swimming faster under appropriately chosen conditions. The activity of the microswimmers is tested in the presence of various concentrations of H_2O_2 to study concentration and illumination effects on the microswimmer speed and mechanism of propulsion. When PHI–Pt and PHI–Au microswimmers are illuminated with visible light at an intensity of 1.6 W/cm^2 in the presence of 2 vol% H_2O_2, they swim with a similar speed of 12.1 ± 0.6 and 11.9 ± 0.4 μm/s, respectively, significantly faster than without illumination (Fig. 3*A*). Hence, also visible light propulsion is possible with H_2O_2 as a fuel. The propulsion under UV illumination is shown in Fig. 3*B*. The PHI–Pt swimmers move with a speed of 13.2 ± 0.9 μm/s already at a concentration of 0.05% H_2O_2, which slightly increases at 0.5% H_2O_2, saturating at 1% (13.6 ± 1.1 and 16.5 ± 1.1 μm/s, respectively; see *SI Appendix*, Fig. S11 for saturation). The maximum speed of the illuminated Pt microswimmers is hence 33% lower than the mean speed with 5% methanol as a fuel.

The PHI–Au microswimmers move faster than the PHI–Pt ones with H_2O_2 (+10% at 0.05% H_2O_2 [14.6 ± 0.8 μm/s] and by +81% at 0.5% [24.6 ± 1.6 μm/s]). Unlike the Pt microswimmers, their speed is significantly increased with increasing the H_2O_2 concentration to 0.5% (+68%), while being 51% faster than with 5% MeOH. The swimming trajectories of the PHI–Pt and PHI–Au microswimmers in 0.5% H_2O_2 are shown in Movies S4 and S5. When the insulating SiO_2 cap is used, the microswimmer speeds are comparable to the metal-capped ones at low H_2O_2 concentrations (10.8 ± 0.7 μm/s at 0.05% H_2O_2). The speed is significantly increased with 0.5% H_2O_2 (19.4 ± 0.9 μm/s, +80%), which remains only 21% below the speed with Au caps and is much higher than with Pt caps at 0.5% H_2O_2 (+43%). Compared to 5% MeOH, the increase is most drastic for the SiO_2-capped

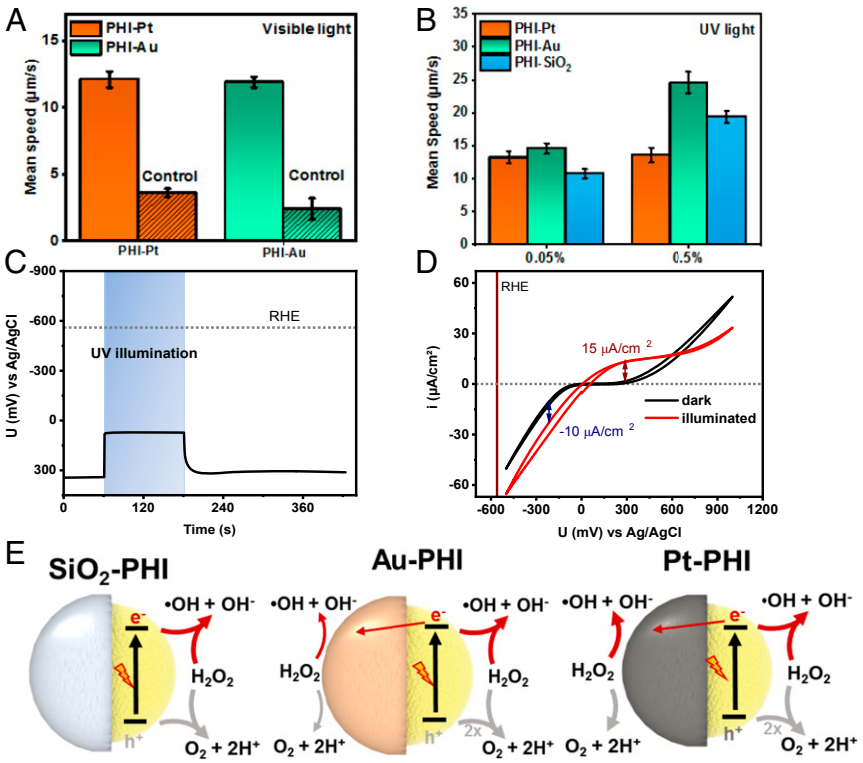

Fig. 3. Characterization of the swimming behavior of PHI-based Janus microswimmers in H_2O_2. (*A*) Average ($n = 25$) mean speed of the visible light-driven PHI–Au and PHI–Pt microswimmers with 2% H_2O_2 as fuel and the control experiment in the dark. (*B*) Average ($n = 25$) mean speed of UV-light propelled PHI-based microswimmers with Pt, Au, and SiO_2 caps at low H_2O_2 concentrations (0.05 and 0.5%) (Movies S4 and S5). (*C*) OCP measurement of PHI nanosheets deposited on FTO in DI water containing 1% H_2O_2 in the dark, under and after UV illumination. (*D*) CV in dark (black curve) and under UV illumination (red curve) with the same conditions as in *C*. (*E*) Schematics illustrating the (competing) major and minor redox reactions with H_2O_2 on both sides of the three PHI-based Janus microswimmers. Reduction reactions (driven by electrons) are indicated by red arrows, whereas the oxidation reactions are highlighted in gray. The electron transfer between the PHI and the metal cap (straight red arrow) indicates a possible self-electrophoretic contribution.

microswimmers (+81%). The fundamentally different trends in propulsion with H_2O_2 compared to MeOH indicate a more complex interplay of the surface reactions, or competitive processes occurring simultaneously on both sides.

Photoelectrochemistry with H_2O_2. The PEC characterization of PHI microswimmers with H_2O_2 relies predominantly on the photoresponse because the dark reduction and oxidation currents from the FTO substrate alone are of comparable size or even stronger than from the electrode containing PHI (*SI Appendix*, Fig. S12 and *Supplementary Note 6*), which cannot be circumvented. Fig. 3*C* contrasts the dark and illuminated OCP of PHI nanosheets on FTO in aqueous 1% H_2O_2. The negative shift from +340 to +70 mV vs. Ag/AgCl upon illumination proves the photoelectron generation, whereas the immediate decay shows that no charge accumulation is possible in the presence of H_2O_2. This is similar to MeOH and O_2 (Fig. 2*D* and *SI Appendix*, Fig. S2), but at overall more positive potentials, since H_2O_2 is reduced more easily than O_2 (*SI Appendix*, *Supplementary Note 6*). Fig. 3*D* illustrates the photocurrents negative and positive of the illuminated OCP value, which remain rather constant at −10 and +15 mA/cm^2, respectively, and illustrate that both the light-induced reduction and oxidation occur very efficiently on PHI, albeit with a slight asymmetry kinetically favoring the oxidation reaction. Similar findings are made with intermittent (chopped) illumination (*SI Appendix*, Fig. S13). Pt-capped PHI Janus microswimmers do not allow for the extraction of photocurrents due to strongly enhanced dark currents by the Pt (*SI Appendix*, Fig. S14). However, the observation of an initially weak negative and subsequently transient positive OCP shift under UV illumination suggests the major photoreaction on PHI still being the H_2O_2 oxidation, while Pt subsequently contributes more to the H_2O_2 reduction (*SI Appendix*, Fig. S15). This case is discussed in more detail in *SI Appendix*, *Supplementary Note 7*.

These findings help us pinpoint the propulsion mechanism. The PHI Janus microswimmer propulsion appears to occur predominantly due to photogenerated electrons and holes on the PHI surface, which drive redox reactions with H_2O_2 at significantly faster kinetics compared to MeOH and dissolved O_2 due to lower reaction overpotentials and, consequently, higher currents on the PHI hemisphere. Hence, the pure symmetry-breaking propulsion mechanism (self-diffusiophoresis) in the PHI–SiO_2 system leads to enhanced MSD in H_2O_2 with respect to MeOH. Au and especially Pt, however, are redox-active materials supporting the disproportionate decomposition of H_2O_2 (48), and Pt is electrochemically much more active than Au, FTO, or PHI, as evidenced by CV measurements (*SI Appendix*, Fig. S16). Consequently, competing reactions at both hemispheres of the Janus microswimmer, effectively lifting the symmetry breaking necessary for propulsion, can slow down the Janus particle under illumination in the presence of a metal cap (49). Therefore, the propulsion with Pt caps is decreased over Au (Fig. 3*B*) where the self-catalyzed and possibly thermally enhanced decomposition of H_2O_2 is less pronounced by more than two orders of magnitude (48).

The light-induced photocatalytic Janus particle propulsion with metal caps thus appears to mainly originate from the PHI

hemisphere, like in the SiO_2 case. A slight increase in swimming speed with Au can again be attributed to a self-electrophoretic contribution enhancing charge separation at the metal–semiconductor interface, akin to the metal-capped microswimmers in MeOH. A summary of the proposed light-induced propulsion mechanisms, which accounts for the complex interplay of the various competing surface catalytic processes of capped PHI microswimmers, is illustrated in Fig. 3*E* for all three Janus particle cases. An overall summary of the mean speeds of the different PHI-based Janus microswimmers under UV-light illumination in different fuels is shown in Table 1.

Solar Battery Swimming. An intriguing question is whether photocharging of PHI microswimmers—the basis for time-delayed photocatalysis in the dark as well as solar batteries based on PHI (37, 38)—could be used to realize a new propulsion mechanism: sustained swimming of light-driven PHI swimmers in the dark through time-delayed discharge, which we call "solar battery swimming." However, the presence of ambient oxygen or H_2O_2, which act as electron scavengers on the PHI surface, would intuitively be expected to hinder charge accumulation of electrons in the conduction band of PHI. A way to circumvent this problem is to charge the bulky Janus particle from inside, making use of sluggish electron transfer kinetics within PHI (from the inside to the surface) for delayed propulsion in the dark (37, 38).

As described before, the surface reactions on the Pt and PHI hemispheres in PHI–Pt Janus microswimmers are in strong competition in H_2O_2, which is not beneficial for fast light-driven propulsion. However, the H_2O_2 decomposition reaction on the Pt surface becomes asymmetric if electrons are transferred away from Pt, as reported for Pt–Au nanorods where the Au hemisphere acts as an acceptor and drives the reduction reaction (50, 51). Translating this effect to Pt–PHI microswimmers could enable electron transfer from Pt to photoexcited PHI, thus leading to hole quenching near the PHI–Pt interface and hence charge accumulation on PHI. We thus studied the propulsion behavior of PHI–Pt microswimmers at 1% H_2O_2 concentrations in more detail, i.e., before, during, and after illumination for different prior illumination times, as shown in Fig. 4. Fig. 4*A* visualizes the instantaneous speed of the microswimmers during an off/on/off cycle, which can be observed in Movie S6. Initially, when the light is off for 7 s, the microswimmers show enhanced Brownian motion due to the surface reaction of Pt with H_2O_2. When the light is turned on for 7 s, the swimmers increase their speed and swim ballistically due to reactions enabled by photogenerated charges, as described earlier. When the light is switched off again for 7 s, however, the swimmers continue to show ballistic motion, hence more directional propulsion in the dark, which is faster than the initial Brownian motion. Hence, the PHI–Pt Janus particle can actually be charged by light while increasing its swimming speed ballistically, which leads to enhanced and lasting propulsion in the dark. Fig. 4*B* illustrates this continuous solar battery swimming process on longer timescales with 5 s of photocharging. The total instantaneous displacement of the microswimmers before, during, and after illumination is illustrated in Fig. 4*C*. The solar battery displacement describes the enhancement in the total instantaneous displacement after illumination on top of the Brownian motion prior to illumination, highlighting that the microswimmers travel much faster and further after illumination than they would have done without it. The ballistic swimming during the dark is shown in orange-color regions in Fig. 4 *B* and *C* (293 μm solar battery displacement in 120 s, which is 2.36 times further than the expected passive Brownian motion in the same duration prior to illumination). The particle trajectory is shown in Fig. 4*D*. Overall, a 5 s period of charging results in 120 to 160 s of enhanced MSD until the swimmers are discharged. This corresponds to a 24 to 32 times increased propulsion period compared to the illumination time. The light-induced enhanced motion as well as its decay is further shown in Movie S7. To further study the solar battery swimming behavior and the relationship between charging and discharging times, we measured the solar battery swimming after 10 and 30 s of prior illumination (see *SI Appendix*, Fig. S17), for instantaneous speeds and total instantaneous displacements for the overall processes). For 10-s illumination, we observe the solar battery swimming effect for ∼400 s (6.7 min), which is ∼40 times longer than the initial charging time, with a solar battery displacement of 767 μm (2.2 times further than the expected passive Brownian displacement in the same duration prior to illumination). As the charging time is increased to 30 s, we observe that the swimming slows down after 800 s, which is about 27 times longer than the initial charging time. However, they continue to swim ballistically up to half an hour and some even beyond, opposite to the non-ballistic Brownian displacement, which is therefore only local without prior illumination. Such an observation indicates that the discharging continues without significantly affecting the swimming speed directly. The total solar battery displacement is 3,580 μm in 27 min (2.16 times further than the passive Brownian displacement in the same duration prior to illumination). The summarized solar battery swimming durations for 5, 10, and 30 s prior illumination times and their respective solar battery displacements are shown in Fig. 4 *E* and *F*, respectively.

In order to realize such a solar battery swimming effect, the electron accumulation process on the PHI during the illumination period, akin to the photocharging occurring prior to "dark photocatalysis" (37, 38), requires faster charging of the PHI compared to the intrinsic discharge rate of electrons driving self-diffusiophoresis or self-electrophoresis. Therefore, a high and asymmetric reaction rate on the Pt side is thus required that quenches the holes on PHI as shown in Fig. 4*G* on the *Left*. Alternatively, the slow electron transfer kinetics from the charged PHI volume to the Pt surface, together with the fast surface reaction on the Pt side, may be the reason for the time-delayed discharge of the PHI particle after the illumination period. In any case, the drift of accumulated charge carriers to the surface enables the photocapacitive, enhanced motion without the presence of light, as shown on Fig. 4*G* on the *Right*, despite conditions that are not beneficial for charge accumulation per se.

Summary and Conclusion

We have studied the propulsion of carbon nitride-based light-driven microswimmers and demonstrate light-induced photocapacitive swimming under dark conditions, which originates

Table 1. Mean speed results of different PHI-based Janus microswimmers under illumination with different fuels added to DI water

Fuel type	PHI–Pt, μm/s	PHI–Au, μm/s	PHI–SiO_2, μm/s
Pure DI water (1.9 W/cm^2 at 365 nm)	10.4 ± 0.6	9.1 ± 0.6	8.6 ± 0.7
Methanol (5 vol%, 1.9 W/cm^2 at 365 nm)	20.4 ± 1.3	16.3 ± 1.4	10.7 ± 0.5
H_2O_2 (0.05 vol%, 1.9 W/cm^2 at 365 nm)	13.2 ± 0.9	14.6 ± 0.8	10.8 ± 0.7
H_2O_2 (0.5 vol%, 1.9 W/cm^2, at 365 nm)	13.6 ± 1.1	24.6 ± 1.6	19.4 ± 0.9
H_2O_2 (2.0 vol%, 1.4 W/cm^2 at 470 nm)	12.1 ± 0.6	11.9 ± 0.4	—

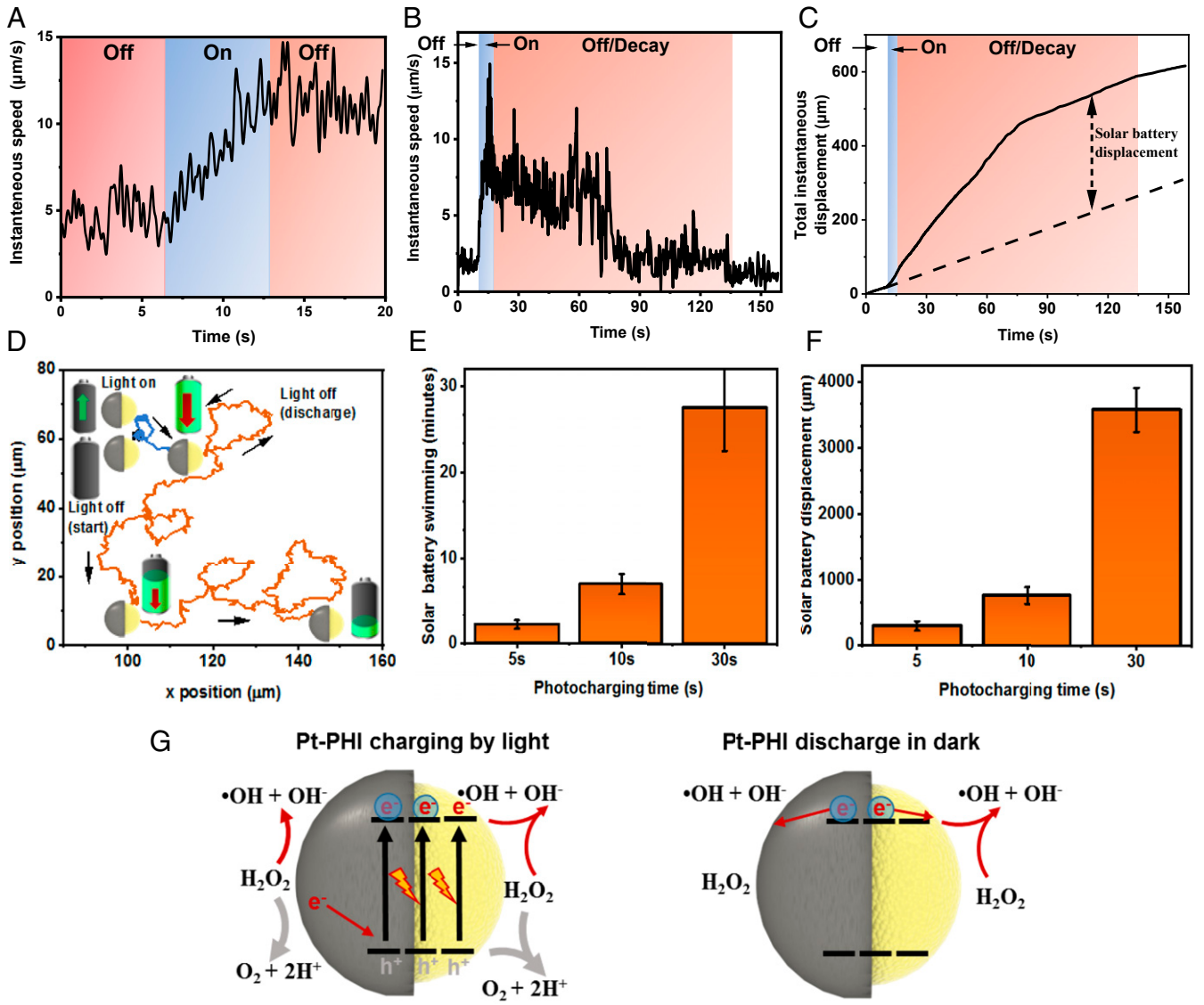

Fig. 4. Light-enhanced swimming during and after UV illumination on PHI–Pt Janus microswimmers in H_2O_2. (*A*) Continuous increase in swimming speed of a PHI–Pt microswimmer with 1% H_2O_2 under UV illumination (blue color), which leads to enhanced propulsion even after illumination is turned off (orange color) (Movie S6). (*B*) Solar battery swimming after 5 s of illumination, which leads to light-induced enhanced motion after UV illumination for periods up to 120 s (shown in orange). See Movie S7 for the swimming. The data represent an averaged instantaneous speed (n = 15). (*C*) Microswimmer total instantaneous displacement (distance traveled) over time extracted from *B*. Dashed line: Total displacement in dark without illumination, solar battery displacement (calculated as the difference between total instantaneous displacement without any and after illumination, both in the dark) is 293 μm in 120 s. (*D*) Corresponding particle trajectory in the dark prior to illumination (0 to 10 s, in black), under illumination (10 to 15 s, in blue), and during solar battery swimming in the dark (15 to 120 s, in orange). The arrows indicate the direction of the trajectory. (*E*) Summary of solar battery swimming durations for 5, 10, and 30 s of prior illumination, respectively. For 30 s of illumination, the end of the solar battery swimming is beyond 30 min for some particles and therefore cannot be measured (hence, the error bar is open toward the top). (*F*) Summary of the total enhanced solar battery displacements for 5, 10, and 30 s of prior illumination, extracted from their instantaneous speeds (*SI Appendix*, Fig. S17). (*G*) Schematic representation of the proposed reaction scheme enabling the solar battery charging mechanism on PHI and the subsequent discharge process enabling solar battery swimming in the dark (same color code as Fig. 3*E*).

from a solar battery functionality in poly(heptazine imide). The PHI–Janus microswimmers show efficient light-induced propulsion under visible light and UV illumination using both alcohols and H_2O_2 as fuels. Assisted by PEC analysis, we elucidate the surface reactions being responsible for the predominantly self-diffusiophoretic propulsion with different caps (Pt, Au, and SiO_2) in the presence of MeOH and H_2O_2 under ambient conditions. We find that PHI–Pt Janus microswimmers swim the fastest with water and alcohol as fuel, whereas PHI–Au ones, followed by PHI–SiO_2 ones, show the fastest propulsion with H_2O_2 as fuel (Table 1). Opposed to the mainstream assumption, we find that hydrogen is not evolved during the photocatalytically induced propulsion under ambient conditions, but oxygen serves as electron scavenger with alcohol donors used as fuels when Pt or Au are used as cocatalysts, even for the most widely used photocatalyst TiO_2. With H_2O_2, unexpected propulsion trends with different caps can be explained by competing surface reactions on both hemispheres. This interplay of different surface processes can be exploited to realize photocharging on PHI–Pt Janus microswimmers at H_2O_2 concentrations of 1% or above, enabling continued enhanced propulsion in the dark for ~40 times longer than the initial illumination period. Some

particles show ballistic swimming beyond half an hour in the dark, after only 30 s of prior illumination. This first observation of a solar battery swimming process is based on the dual light absorption and energy storage capability of PHI, akin to dark photocatalysis. However, its realization is a product of careful interfacial reaction studies and their rational tuning in order to enable the simultaneous charging and discharging of the PHI volume to achieve continued propulsion in the dark.

The unique properties of PHI-based microswimmers make them particularly promising for potential medical (e.g., targeted drug delivery) and environmental remediation applications, due to their sensitivity to visible light, their soft organic nature, and the possibility to use biocompatible caps such as Au or SiO_2. The solar battery swimming effect is anticipated to open new capabilities in diverse applications, where micro/nanomachines need to operate without continuous external fuel supply, and where environmentally or biologically benign materials are required. Finally, the charging effect reported here opens the door to the creation of autonomous systems with built-in energy storage capabilities, since PHI cannot only drive redox reactions in a time-delayed manner, but also provide an electrical potential, akin to a battery.

Materials and Methods

PHI Synthesis. PHI was synthesized according to a procedure described in the literature (32, 37). In brief, melamine (5.0 g) was heated in a tube furnace in a quartz glass boat to 550 °C for 12 h with a heating rate of 5 °C/min under argon (Ar) flow. After cooling to ambient temperature, a yellow powder (2.0 to 2.5 g) was obtained. A total of 1.5 g of this product (Melon) was thoroughly ground with KSCN (3.0 g), which was heated overnight to 140 °C in vacuum to evaporate water. The mixture was heated in a tube furnace in an aluminum oxide (Alox) boat to 400 °C for 1 h and 500 °C for 30 min with a heating rate of 30 °C/min under Ar flow. The Alox boat with the PHI was sonicated two times for 15 min in 80 mL of water to disperse the yellow product. This suspension was washed six times with DI water by centrifugation (20,000 rpm). The insoluble product was dried in vacuum at 60 °C overnight.

PHI Characterization. SEM images of the Janus microswimmers were captured by a Zeiss Merlin SEM with an Oxford Ultim Extreme EDS. For the Janus metal cap deposition, a Nano 36 DC sputtering machine from Kurt Lesker was used. In order to capture the swimming of the microswimmers, a Zeiss Axio A1 inverted optical microscope was used. A Thorlabs M365L2 UV lamp (365 nm) was used for illumination through the inverted microscope. The videos were recorded from the microscope using a LD Plan-NeoFluar 40× objective lens and Axiocam 503 CCD camera at 62 frames per second (fps). In the case of solar battery swimming experiments, the videos were recorded at 10 fps for 5- and 10-s prior illumination and at 5 fps for 30-s prior illumination. The swimming behavior of the microswimmers was systematically investigated by 2D MSD analysis on the captured videos for 15 s using a custom MATLAB code. All fuel concentrations are in volume percentage. In Fig. 4*B*, the instantaneous data have been smoothened by a fast Fourier transform filter with a cutoff frequency at 3.1 Hz after averaging.

The absorptance spectra of these samples were measured with a double monochromator spectrophotometer (Edinburgh Instruments; FLS-980). The measurements were performed locating the sample in the center of an integrating sphere attached to FLS-980 working in synchronous mode to discern any photoluminescence signal from the PHI particle. The sample suspension was measured in aqueous solution with and without O_2 while being stirred to prevent sedimentation.

PHI-Based Janus Microswimmer Fabrication. To obtain microswimmers of PHI for the microswimmer preparation, 0.3 g of the material was sonicated in 200 mL of DI water in an ice-cooled bath for 2 h, while shaking the suspension by hand every 30 min in addition. The obtained suspension was then centrifuged at 353 rcf for 20 min to agglomerate smaller particles that were used for PEC purposes. The supernatant containing larger particles was removed for the Janus particle fabrication. These were resonicated for 30 min and centrifuged at 1500 rcf. Five hundred microliters of the stock solution with a concentration of 3 mg/mL were suspended in 10 mL of ethanol, followed by further sonication for 30 min. One hundred microliters of the resulting suspension were drop cast onto the glass wafer, resulting in a thin layer of the particles on the substrate. Thirty nanometers of Pt were sputtered on top to form Janus microswimmers. The wafer was then sonicated in water to release the microswimmers that were then used for further experiments. The same procedure was repeated for fabrication of PHI–Au, PHI–SiO_2 (with 20-nm-thick sputtered material, respectively), and the bilayer PHI–Ni–Pt Janus microswimmers used for magnetic propulsion.

Light Intensity Measurements. The spectral irradiance of the illumination in the microscope was measured at the place of the sample chamber with a calibrated Ocean Optics OCEAN-FX-XR1-ES spectrophotometer after attenuation by a neutral density filter. The results (*SI Appendix*, Fig. S2) have been normalized to the filter attenuation and to the spot size of the light beam in the microscope, which was measured to be 2.0 ± 0.5 mm in diameter, resulting in a relative experimental error of 50% after the error propagation calculation. In the case of visible light propulsion, a broad-spectrum white LED is illuminated from the top and a 470-nm light is illuminated through the microscope objective lens. The intensity of the microscope light (2 mW/cm^2 for the control experiments in the dark and 7 mW/cm^2 for imaging during UV illumination) was increased to 20 mW/cm^2 for visible light propulsion. For photocatalytic and PEC experiments, the light intensity was directly measured by a calibrated Thorlabs S310C/PM100D power meter.

Photocatalytic Experiments. Photocatalytic experiments were performed in a double-walled glass reactor with a quartz glass window on top, as previously reported (52). The temperature within the reactor was thermostated by a water cooling jacket to 25 °C. Top illumination of the reactor is performed with a xenon lamp (Newport; 300 W) with a water filter, or by a Thorlabs M365L2 UV lamp. To cut off some of the UV-light, air mass filter (AM 1.5 G) was used in the respective experiments. If not stated otherwise, CN_x Janus microswimmers were suspended in water (9 mL) and methanol (1 mL). Prior to illumination, the head space of the reactor was evacuated and backfilled with Ar six times to remove oxygen. The headspace was periodically analyzed by a gas chromatograph (Thermo Scientific; TRACE GC Ultra) equipped with a thermal conductivity detector using Ar as a carrier gas.

For HER measurements with photodeposited Pt or Au on PHI or TiO_2 (anatase; Sigma-Aldrich; 232033), the same reactor preparation and geometry were used, with full arc illumination by the same Xe lamp, set to 100 mW/cm^2. For photodeposition of the cocatalyst Pt or Au, an optimized amount (8 wt% or 2 wt%) of H_2PtCl_6 or $HAuCl_4$ (Sigma-Aldrich) was added to the suspension before the measurement in argon-containing conditions. After at least 6 h of measurement, the O_2 containing experiment was performed on the same material. The suspension was purged with O_2 through a needle for 20 min while stirring (1 mL of MeOH was added after 15 min to prevent its evaporation), and the reactor was left open for 10 min to equilibrate. In all cases, the HER rate was determined by the average slope after activation over at least 3 h, with a minimum sensitivity of 0.06 μmol H_2/h over 3 h.

PEC Measurements. The PEC measurements were performed in a closed glass reactor equipped with a quartz window for side illumination. An Ag/AgCl reference electrode with saturated KCl (+0.197 V vs. NHE) was used with the different aqueous electrolytes. A Pt wire acted as counter electrode. To remove dissolved oxygen, the electrolyte was purged with >99% pure N_2 or Ar prior to the respective measurement through a porous glass frit for at least 1 h. Electrochemical measurements were recorded and analyzed using an IVIUM CompactStat potentiostat and the IviumSoft software. UV illumination was provided by a Thorlabs M365L2 UV lamp at an operating current of 1.4 mA and a working distance of 20 cm (15 mW/cm^2). PHI was deposited on FTO by drop casting nanosheets as reported previously (38).

Data Availability. All data, materials, and associated protocols that support the findings of this study are shown in *Materials and Methods* and *SI Appendix*.

ACKNOWLEDGMENTS. We thank V. Duppel for SEM and energy-dispersive X-ray spectroscopy imaging and fruitful discussions, and F. Thiel and G. Richter for their support with sputter deposition. Financial support by an ERC Starting Grant (project COF Leaf, Grant No. 639233), the Deutsche Forschungsgemeinschaft via the cluster of excellence "e-conversion" and the Center for NanoScience is gratefully acknowledged by B.V.L. A.J.-S. gratefully acknowledges a postdoctoral scholarship from the Max Planck Society. This work was funded by the Max Planck Society.

1. M. Luo, Y. Z. Feng, T. W. Wang, J. G. Guan, Micro-/nanorobots at work in active drug delivery. *Adv. Funct. Mater.* **28**, 1706100 (2018).
2. M. Sitti, *Mobile Microrobotics*, (MIT Press, Cambridge, MA, 2017).
3. P. Erkoc *et al*., Mobile microrobots for active therapeutic delivery. *Adv. Ther. (Weinh.)* **2**, 1800064 (2019).
4. S. Sánchez, L. Soler, J. Katuri, Chemically powered micro- and nanomotors. *Angew. Chem. Int. Ed. Engl.* **54**, 1414–1444 (2015).
5. R. Dong, Y. Cai, Y. Yang, W. Gao, B. Ren, Photocatalytic micro/nanomotors: From construction to applications. *Acc. Chem. Res.* **51**, 1940–1947 (2018).
6. H. Eskandarloo, A. Kierulf, A. Abbaspourrad, Light-harvesting synthetic nano- and micromotors: A review. *Nanoscale* **9**, 12218–12230 (2017).
7. J. Wang, Z. Xiong, J. Zheng, X. Zhan, J. Tang, Light-driven micro/nanomotor for promising biomedical tools: Principle, challenge, and prospect. *Acc. Chem. Res.* **51**, 1957–1965 (2018).
8. W. E. Uspal, Theory of light-activated catalytic Janus particles. *J. Chem. Phys.* **150**, 114903 (2019).
9. W. Wang, W. Duan, S. Ahmed, T. E. Mallouk, A. Sen, Small power: Autonomous nano- and micromotors propelled by self-generated gradients. *Nano Today* **8**, 531–554 (2013).
10. L. Xu, F. Mou, H. Gong, M. Luo, J. Guan, Light-driven micro/nanomotors: From fundamentals to applications. *Chem. Soc. Rev.* **46**, 6905–6926 (2017).
11. S. Simoncelli, J. Summer, S. Nedev, P. Kühler, J. Feldmann, Combined optical and chemical control of a microsized photofueled Janus particle. *Small* **12**, 2854–2858 (2016).
12. F. Mou *et al*., Light-controlled propulsion, aggregation and separation of water-fuelled TiO_2/Pt Janus submicromotors and their "on-the-fly" photocatalytic activities. *Nanoscale* **8**, 4976–4983 (2016).
13. B. Jang *et al*., Multiwavelength light-responsive Au/B-TiO_2 Janus micromotors. *ACS Nano* **11**, 6146–6154 (2017).
14. C. Chen *et al*., Light-steered isotropic semiconductor micromotors. *Adv. Mater.* **29**, 1603374 (2017).
15. R. Dong *et al*., Visible-light-driven BiOI-based Janus micromotor in pure water. *J. Am. Chem. Soc.* **139**, 1722–1725 (2017).
16. J. Zheng *et al*., Orthogonal navigation of multiple visible-light-driven artificial microswimmers. *Nat. Commun.* **8**, 1438 (2017).
17. X. Zhan *et al*., Enhanced ion tolerance of electrokinetic locomotion in polyelectrolyte-coated microswimmer. *Nat. Commun.* **10**, 3921 (2019).
18. D. Zhou *et al*., Visible-light controlled catalytic Cu_2O–Au micromotors. *Nanoscale* **9**, 75–78 (2017).
19. X. Chen, C. Zhou, W. Wang, Colloidal motors 101: A beginner's guide to colloidal motor research. *Chem. Asian J.* **14**, 2388–2405 (2019).
20. A. M. Pourrahimi *et al*., Catalytic and light-driven ZnO/Pt Janus nano/micromotors: Switching of motion mechanism via interface roughness and defect tailoring at the nanoscale. *Adv. Funct. Mater.* **29**, 1808678 (2019).
21. Y. Hong, M. Diaz, U. M. Córdova-Figueroa, A. Sen, Light-driven titanium-dioxide-based reversible microfireworks and micromotor/micropump systems. *Adv. Funct. Mater.* **20**, 1568–1576 (2010).
22. M. Enachi *et al*., Light-induced motion of microengines based on microarrays of TiO_2 nanotubes. *Small* **12**, 5497–5505 (2016).
23. M. Ni, M. K. H. Leung, D. Y. C. Leung, K. Sumathy, A review and recent developments in photocatalytic water-splitting using for hydrogen production. *Renew. Sustain. Energy Rev.* **11**, 401–425 (2007).
24. F. Mou *et al*., Single-component TiO_2 tubular microengines with motion controlled by light-induced bubbles. *Small* **11**, 2564–2570 (2015).
25. B. Dai *et al*., Programmable artificial phototactic microswimmer. *Nat. Nanotechnol.* **11**, 1087–1092 (2016).
26. V. Sridhar, B.-W. Park, S. Guo, P. A. van Aken, M. Sitti, Multiwavelength-steerable visible-light-driven magnetic CoO-TiO_2 microswimmers. *ACS Appl. Mater. Interfaces* **12**, 24149–24155 (2020).
27. X. Wang *et al*., Fuel-Free Nanocap-Like Motors Actuated Under Visible Light. *Adv. Funct. Mater.* **28**, 1705862 (2018).
28. M. You, C. Chen, L. Xu, F. Mou, J. Guan, Intelligent micro/nanomotors with taxis. *Acc. Chem. Res.* **51**, 3006–3014 (2018).
29. Y. Wang, X. Wang, M. Antonietti, Polymeric graphitic carbon nitride as a heterogeneous organocatalyst: From photochemistry to multipurpose catalysis to sustainable chemistry. *Angew. Chem. Int. Ed. Engl.* **51**, 68–89 (2012).
30. Y. Cui *et al*., Metal-free activation of H_2O_2 by g-C_3N_4 under visible light irradiation for the degradation of organic pollutants. *Phys. Chem. Chem. Phys.* **14**, 1455–1462 (2012).
31. B. V. Lotsch *et al*., Unmasking melon by a complementary approach employing electron diffraction, solid-state NMR spectroscopy, and theoretical calculations—structural characterization of a carbon nitride polymer. *Chemistry-A European Journal* **13**, 4969–4980 (2007).
32. V. W. Lau *et al*., Rational design of carbon nitride photocatalysts by identification of cyanamide defects as catalytically relevant sites. *Nat. Commun.* **7**, 12165 (2016).
33. Z. Ye, Y. Sun, H. Zhang, B. Song, B. Dong, A phototactic micromotor based on platinum nanoparticle decorated carbon nitride. *Nanoscale* **9**, 18516–18522 (2017).
34. K. Villa, C. L. Manzanares Palenzuela, Z. Sofer, S. Matějková, M. Pumera, Metal-free visible-light photoactivated C_3N_4 bubble-propelled tubular micromotors with inherent fluorescence and on/off capabilities. *ACS Nano* **12**, 12482–12491 (2018).
35. H. Schlomberg *et al*., Structural insights into poly(heptazine imides): A light-storing carbon nitride material for dark photocatalysis. *Chem. Mater.* **31**, 7478–7486 (2019).
36. Y. Markushyna *et al*., Green radicals of potassium poly(heptazine imide) using light and benzylamine. *J. Mater. Chem. A Mater. Energy Sustain.* **7**, 24771–24775 (2019).
37. V. W. Lau *et al*., Dark photocatalysis: Storage of solar energy in carbon nitride for time-delayed hydrogen generation. *Angew. Chem. Int. Ed. Engl.* **56**, 510–514 (2017).
38. F. Podjaski, J. Kröger, B. V. Lotsch, Toward an aqueous solar battery: Direct electrochemical storage of solar energy in carbon nitrides. *Adv. Mater.* **30**, 1705477 (2018).
39. V. Sridhar, B. W. Park, M. Sitti, Light-driven Janus hollow mesoporous TiO_2-Au microswimmers. *Adv. Funct. Mater.* **28**, 1704902 (2018).
40. A. Savateev *et al*., Potassium poly(heptazine imides) from aminotetrazoles: Shifting band gaps of carbon nitride-like materials for more efficient solar hydrogen and oxygen evolution. *ChemCatChem* **9**, 167–174 (2017).
41. A. Savateev, D. Dontsova, B. Kurpil, M. Antonietti, Highly crystalline poly(heptazine imides) by mechanochemical synthesis for photooxidation of various organic substrates using an intriguing electron acceptor—elemental sulfur. *J. Catal.* **350**, 203–211 (2017).
42. H. Kasap *et al*., Solar-driven reduction of aqueous protons coupled to selective alcohol oxidation with a carbon nitride-molecular Ni catalyst system. *J. Am. Chem. Soc.* **138**, 9183–9192 (2016).
43. X. Wang *et al*., Fuel-free nanocap-like motors actuated under visible light. *Adv. Funct. Mater.* **28**, 1705862 (2018).
44. R. Dong, Q. Zhang, W. Gao, A. Pei, B. Ren, Highly efficient light-driven TiO_2-Au Janus micromotors. *ACS Nano* **10**, 839–844 (2016).
45. T. Maric, M. Z. M. Nasir, R. D. Webster, M. Pumera, Tailoring metal/TiO_2 interface to influence motion of light-activated Janus micromotors. *Adv. Funct. Mater.* **30**, 1908614 (2020).
46. M. Z. Rahman *et al*., A benchmark quantum yield for water photoreduction on amorphous carbon nitride. *Adv. Funct. Mater.* **27**, 1702384 (2017).
47. Y. Nosaka, A. Y. Nosaka, Generation and detection of reactive oxygen species in photocatalysis. *Chem. Rev.* **117**, 11302–11336 (2017).
48. D. W. McKee, Catalytic decomposition of hydrogen peroxide by metals and alloys of the platinum group. *J. Catal.* **14**, 355–364 (1969).
49. H. Šípová-Jungová, D. Andrén, S. Jones, M. Käll, Nanoscale inorganic motors driven by light: Principles, realizations, and opportunities. *Chem. Rev.* **120**, 269–287 (2020).
50. M. Kuron, P. Kreissl, C. Holm, Toward understanding of self-electrophoretic propulsion under realistic conditions: From bulk reactions to confinement effects. *Acc. Chem. Res.* **51**, 2998–3005 (2018).
51. W. Wang, T.-Y. Chiang, D. Velegol, T. E. Mallouk, Understanding the efficiency of autonomous nano- and microscale motors. *J. Am. Chem. Soc.* **135**, 10557–10565 (2013).
52. V. W. Lau *et al*., Low-molecular-weight carbon nitrides for solar hydrogen evolution. *J. Am. Chem. Soc.* **137**, 1064–1072 (2015).